JOURNAL OF GEOPHYSICAL RESEARCH, VOL. 93, NO. B4, PAGES 2955–2966, APRIL 10, 1988

Three-Dimensional Flow and Temperature Perturbations Due to a Transform Offset: Effects on Oceanic Crustal and Upper Mantle Structure

JASON PHIPPS MORGAN[1]

Scripps Institution of Oceanography, Institute of Geophysics and Planetary Physics, La Jolla, California

DONALD W. FORSYTH

Department of Geological Sciences, Brown University, Providence, Rhode Island

Systematic changes in seafloor depth, crustal structure, and crustal geochemistry can occur within 30 km of a fracture zone. The seafloor gradually deepens roughly 1 km within 30 km from the fracture zone, the crust may be thinner than crust created far from a fracture zone, and systematic compositional differences are observed between basalts erupted near and far from fracture zones. We call these effects the transform fault effect (TFE). To investigate the physical processes responsible for the TFE, a general numerical method is developed to solve for the three-dimensional flow and thermal structure beneath a mid-ocean spreading center. This model is applied to study an idealized spreading center consisting of a 100 km transform fault offsetting two ridge segments spreading at rates of 1, 2, and 4 cm/yr. Using an adiabatic melt relation and our flow and temperature calculations, we find the distribution of melt production beneath the spreading center. Finally, a porous flow model of melt migration within a spreading center is developed to assess the possible effects of melt migration on oceanic crustal structure. We find that the expected topographic effects caused by mantle density variations associated with cooling near a transform offset are far smaller than the observed 1 km seafloor deepening within 30 km of a fracture zone. While significant compositional upper mantle heterogeneity due to lower degrees of partial melting will be associated with fracture zones, isostatic compensation of ridge parallel upper mantle heterogeneity also does not seem a likely cause for observed seafloor deepening toward a fracture zone. Crustal thickness variation is a good candidate to explain this seafloor deepening. Several kilometers of crustal thinning can plausibly occur within 30 km of a fracture zone. This thinning is due to both perturbations in melt migration at a transform offset with melt preferentially migrating toward the center of a spreading segment and perturbations in melt production near a transform offset caused by lower upwelling rates near the transform. The major influence of a transform offset on melting beneath a ridge-transform spreading center is due to the muting effect of a transform offset on upwelling beneath the ridge-transform intersection; lower rates of upwelling lead to lower amounts of melt production within a broad region near the transform. Our results (weakly) support Bender, Langmuir, and Hansen's petrological investigations of along-axis variability in the depth of melting. They found a greater average depth of melting for basalts erupted toward the center of a spreading segment versus basalts erupted near a transform fault. Our results suggest that the actual depth of the beginning of melting along a spreading center is not strongly affected by a transform offset but that melt production occurs over a larger depth interval toward the center of a spreading segment. Thus melt production variations alone tend to produce a trend opposite to that found by Bender, Langmuir, and Hansen. However, variations in melt migration can produce the trend found by Bender, Langmuir, and Hansen; melt created at greater depths beneath a transform will migrate further toward the center of a spreading segment than melt created at shallow depths. Present calculations are inconclusive in showing whether the effects of melt production or melt migration dominate at a ridge-transform intersection.

INTRODUCTION

Approaching a fracture zone along an isochron, the seafloor gradually deepens roughly 1 km within 30 km from the fracture zone [*Fox and Gallo*, 1984; *White et al.*, 1984; *Mutter and Detrick*, 1984]. Within a median valley this deepening is even more pronounced, with 2 km or more of along-axis seafloor deepening toward a transform fault [*Parmentier and Forsyth*, 1985]. Dynamic mechanisms can explain part of this effect within the median valley [*Parmentier and Forsyth*, 1985]. However, dynamic mechanisms for relief within the median valley do not predict this persistent seafloor deepening on older ocean seafloor, since the dynamic forces producing a depression within the median valley induce opposing forces producing uplift of the rift mountains so that the regional dynamic vertical force distribution is zero.

Seafloor near fracture zones also has a distinct chemical and crustal signature. The crust may be thinner than crust created far from a fracture zone [*Detrick and Purdy*, 1980; *Mutter and Detrick*, 1984; *White et al.*, 1984; *Cormier et al.*, 1984]. Incompatible element abundances also tend to be higher in basalts erupted near fracture zones [*Hekinian and Thompson*, 1976; *Bender et al.*, 1984]. *Bender et al.* [1984] called the systematic geochemical changes they observed in basalts

[1]Now at Department of Earth, Atmospheric, and Planetary Sciences, Massachusetts Institute of Technology, Cambridge.

Paper number 6B6176.
0148-0227/88/006B-6176$5.00

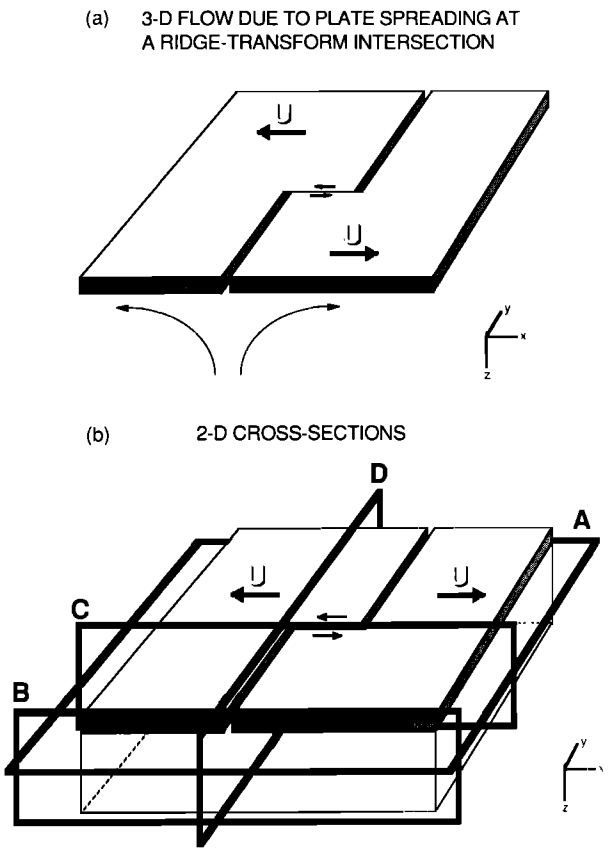

Fig. 1. (*a*) Ridge-transform-ridge spreading center geometry and (*x*, *y*, *z*) coordinate system used in flow and temperature models. Transform fault is marked as arrow couple, indicating shear. We model upwelling induced by spreading of constant thickness lithosphere (shaded in figure). (*b*) Spreading center geometry and location of two-dimensional cross-sections.

erupted near a transform fault the transform fault effect or TFE. In this paper, TFE will be used to denote both systematic geophysical and geochemical changes associated with a transform offset. *Fox and Gallo* [1984] speculated that heat transfer from asthenosphere rising at a ridge axis to older, colder lithosphere on the other side of the transform fault, plus associated reduced melting, may be responsible for all these phenomena. Here we shall quantitatively evaluate this hypothesis.

In this paper we develop a flow model for a mid-ocean ridge-transform-ridge spreading center and explore some of the effects on mid-ocean ridge upwelling due to a transform fault offsetting two ridge segments. With this flow model, we assess the relative importance of convection and conduction for lateral heat transport near a transform. Using an adiabatic pressure release melt relation and our calculated flow and temperature fields, we also explore the effects of a transform fault on melt production beneath a spreading center. Finally, we also assess the possible effects of melt migration on oceanic crustal structure.

Flow Model

Our previous three-dimensional thermal model of a ridge-transform-ridge spreading system assumed a flow structure that was everywhere vertical within the upwelling region and everywhere parallel to the plate spreading direction away from the upwelling zone [*Forsyth and Wilson*, 1984]. Thus this model could only examine lateral heat conduction toward the transform fault. Here we will consider a semi-analytical solution for uniform viscosity mantle flow in a half-space beneath constant thickness lithosphere which is, in essence, a three-dimensional analog to the two-dimensional plate spreading solution [*Batchelor*, 1967, p. 225] used in *Reid and Jackson*'s [1981] thermal model of a spreading center. We can solve for the plate-driven (creeping) flow of a uniform viscosity mantle beneath an arbitrary geometry ridge-transform-ridge spreading center via a Fourier series decomposition. Note that this passive upwelling due to plate spreading does not produce stress-supported topography [*Phipps Morgan et al.*, 1987]. The solution for a given Fourier harmonic and details of the solution method are presented in Appendix A. We use a standard fast Fourier transform algorithm to solve for the flow induced by prescribed surface motions. Part of the power of this approach is that we may readily solve for the flow beneath a complex geometry spreading center which may more realistically include multiple short transform offsets or short spreading segments. However, in this study we will focus on a simple case of the flow field due to a single 100-km-long transform fault offsetting two ridge axes (see Figure 1). A 512 x 256 velocity grid is calculated for each depth with 512, 1.5625-km-spaced, along-axis grid points and 256, 2-km-spaced, spreading direction grid points. This results in an effective periodic transform fault spacing of 400 km. The velocity solutions are accurate for depths greater than the grid spacing increment or greater than 1-2 km in this case.

Figures 2 and 3 show flow vectors and contours of flow magnitude for a few representative slices through the spreading center. Note in particular the smoothing of the transform offset on vertical upwelling with increasing depth beneath the spreading center (Figure 3*d*) and the extent of horizontal flow toward the ridge axis from the old side of the transform fault that is induced by the slower upwelling near the transform offset. The maximum along-axis horizontal flow velocities occur at the ridge-transform intersection and are roughly 20% of the spreading velocity or 33% of the maximum upwelling velocity. The pattern of flow is independent of the absolute value of the (uniform) mantle viscosity. Except for a constant scaling factor, the flow pattern is also independent of the spreading rate. However, the temperature field will depend on the spreading rate.

Thermal Model

Upwind finite differences were used to solve for the temperature field associated with the above flow field within a rectangular parallelepiped region extending 100 km beneath the ridge axis, 200 and 100 km to each side of the transform fault, and 300 and 200 km to each side of the ridge axes. Variable grid spacing was used, with the densest grid spacing in regions with strong flow or temperature gradients. Temperature solutions were found for a constant transform offset of 100 km and half-spreading rates of 1, 2, and 4 cm/yr. The mantle temperature at 100-km depth is assumed to be 1310°C and at the surface is 0°C. The sides of the box are assumed to have no horizontal temperature gradient (symmetry planes). Details of our numerical method and convergence tests are given in Appendix B. We expect our temperature solutions to be accurate to within better than 10-20°C except within a 30-km radial distance from each ridge axis, where both temperature and flow gradients are high. In this region our solutions reach a

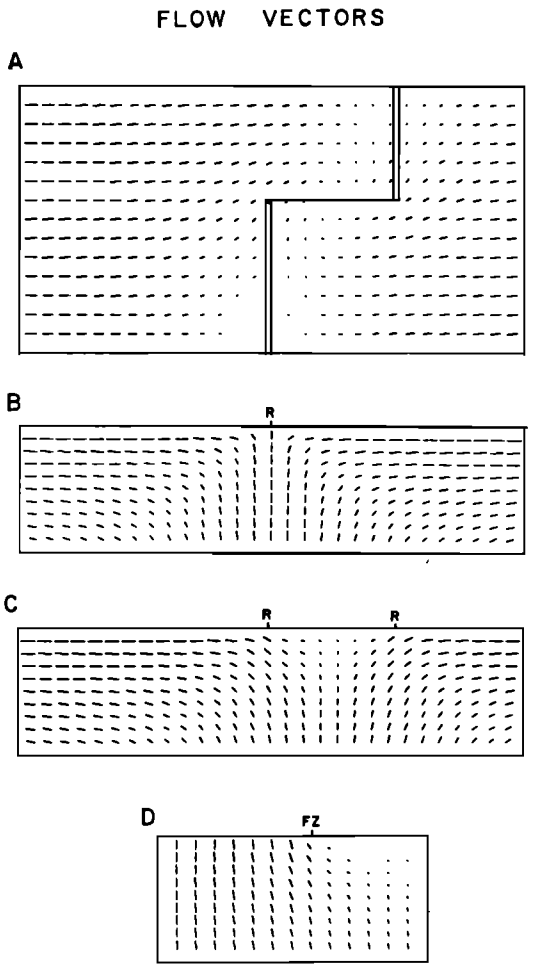

Fig. 2. Cross sections of flow vectors at a ridge-transform-ridge spreading center with a 100-km transform offset. (See Figure 1*b* for schematic location of cross sections.) (*a*) Horizontal cross section at a depth of 13 km. (*b*) Vertical cross section parallel to the transform at y = -200 km, far from the transform fault (y = 0). (*c*) Vertical cross section along the transform fault (y = 0). (*d*) Vertical cross section perpendicular to the transform through the ridge axis (x = 0).

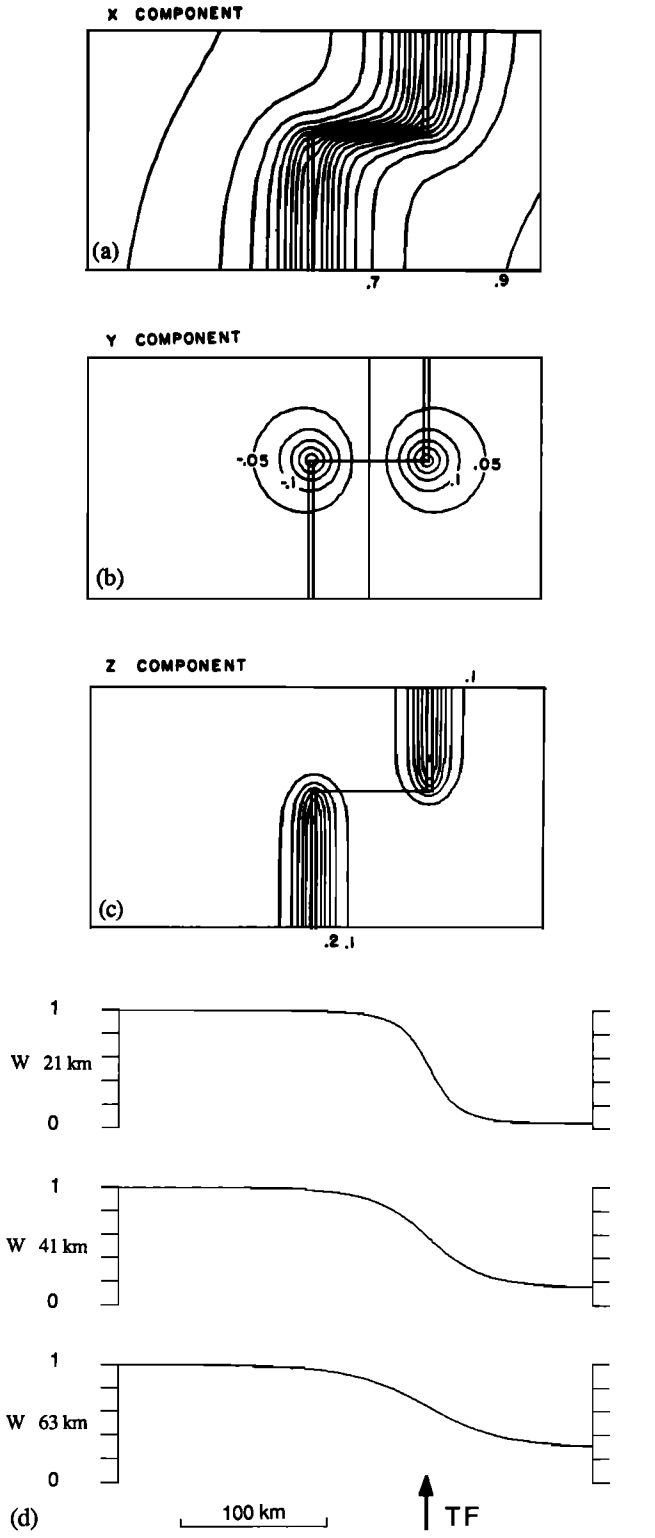

Fig. 3. Contours of u, v, w velocity component magnitude at a ridge-transform-ridge spreading center with a 100-km transform offset. (*a*) Contours of u (x direction) velocity magnitude at a depth of 13 km. (*b*) Contours of v (y direction) velocity at a depth of 13 km. (*c*) Contours of w (z direction) velocity at a depth of 13 km. (*d*) Upwelling (w) velocity magnitude directly beneath a ridge axis at depths of 21, 41, and 63 km. TF marks location of transform fault, upwelling to the left of the transform occurs beneath old lithosphere. Upwelling is normalized by $2U/\pi$, the ridge axis upwelling velocity if no transform offset were present, where U is the half-spreading rate. Note the broadening of upwelling with increasing depth beneath the spreading center.

maximum error of 100°C 10 km directly beneath the ridge axis and have a 1-2 km systematic overdeepening of each 100° isotherm. We have neglected the increased heat transfer and cooling from hydrothermal circulation in this study, as it will only affect the temperature distribution within 10 km from the surface. Only in a study of local ridge axis temperature structure, perhaps with a transient intrusion and cooling cycle, would hydrothermal circulation play a significant role in shaping the thermal structure. Since we are studying the large-scale, steady state, deep thermal anomalies associated with a transform offset, these additional complexities are somewhat irrelevant. In any case, our neglect of hydrothermal circulation renders our calculated near ridge axis temperatures somewhat irrelevant, with actual errors larger than our calculated formal error due to neglect of this process and of the transient nature of small-scale intrusion and cooling.

Figure 4 shows a representative temperature calculation for a half-spreading rate of 1 cm/yr and a transform offset of 100 km. Upper mantle temperatures cool several hundred degrees within 25 km of the transform fault. While solely conductive

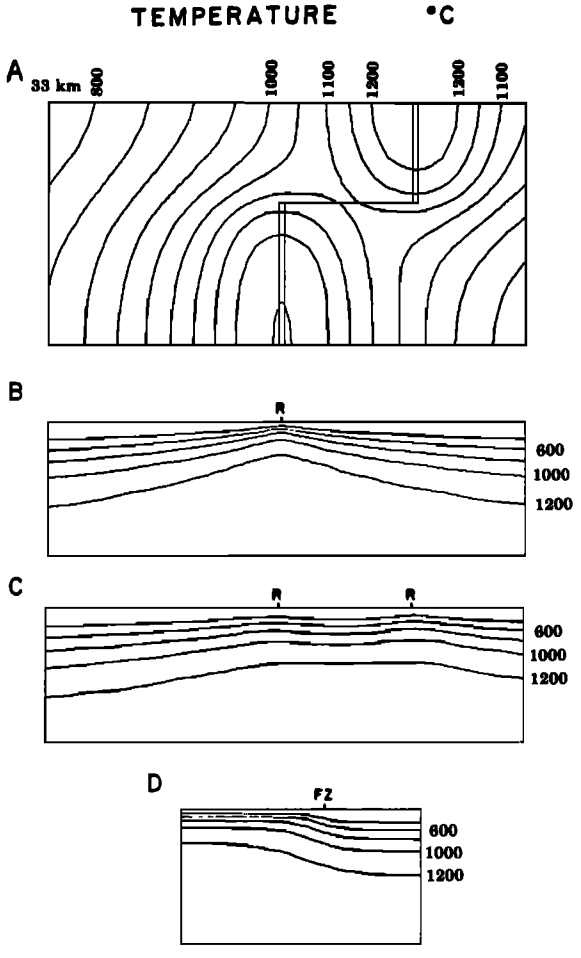

Fig. 4. Representative thermal calculation for a spreading system with a 100-km transform fault and half-spreading rate of 1 cm/yr. Same cross sections as in Figure 2 (or 1*b*). (*a*) Horizontal cross section is at a depth of 33 km.

lateral heat transport results in TFE cooling only ±15 km from the transform fault [*Forsyth and Wilson*, 1984], advective heat transport extends the region of TFE cooling to ±25 km from the transform fault. Mantle density variations caused by transform cooling generate very little surface topography. To estimate the magnitude of this topography, we will assume that vertical columns of mantle are in isostatic equilibrium at 100 km depth. The resulting topographic variation Δ due to thermal contraction is $\rho_m/(\rho_m - \rho_w) \int_z \alpha \Delta T \, dz$, with the volumetric thermal expansion coefficient $\alpha = 3 \times 10^{-5}$/°C. Figure 5 shows the anomalous thermal topography predicted for a transform fault offset of 100 km and spreading rates of 1, 2, and 4 cm/yr (subtracting the topographic effect of plate cooling with age). Maximum anomalous thermal topography is only ±300 m at the ridge-transform intersection and rapidly dies off away from the ridge axis. To first order, thermal conduction does not create a net downwarp near a fracture zone; the uplift on the older side of the fracture zone balances the downwarp on the younger side. With time, both sides converge in elevation as further cooling occurs. These results strongly suggest that thermal contraction is not only incapable of producing the observed median valley deepening toward a fracture zone [*Forsyth and Wilson*, 1984] but is also incapable of producing the observed long-lived seafloor deepening toward a fracture zone. Melting beneath the ridge axis (see next section) will result in mantle temperatures remaining at the solidus in regions of melting. This will tend to reduce our calculated temperature variation away from the transform fault and result in smaller thermal topographic variations than shown in Figure 5. As long as only a small melt fraction is trapped in the melting region, the topographic effects of a low-density melt phase will be negligible. Any mantle strength or flexural rigidity of the lithosphere that distributes the (regionally cancelling) forces caused by mantle density variations due to thermal expansion will also result in even smaller topographic anomalies than we calculate.

However, although temperature variations near a transform will not directly produce sufficient topographic anomalies, temperature (and flow) perturbations may have a strong effect on the degree of melting near a transform fault. Variations in the degree of melting beneath a ridge axis may affect both the along-axis crustal structure and the along-axis composition of the residual upper mantle – both of which may produce topographic deepening toward a transform. Melt production and melt migration in a multicomponent, multiphase material can be extremely complicated processes. Since we are interested here in obtaining first-order constraints on the plausible scale of along-axis crustal and upper mantle variation, we will use simple physical idealizations of these processes. We hope that while our quantitative results may differ from the results of more complete models, we will still obtain a good qualitative understanding of the possible effects of these processes.

Melt Production Beneath a Ridge Axis

The observed generally uniform composition of erupted basalts along a ridge axis suggests that melting is an isochemical process (melting occurs at the same eutectic throughout the melt region). We assume this is true and hence that the latent heat of melting is constant for any degree of

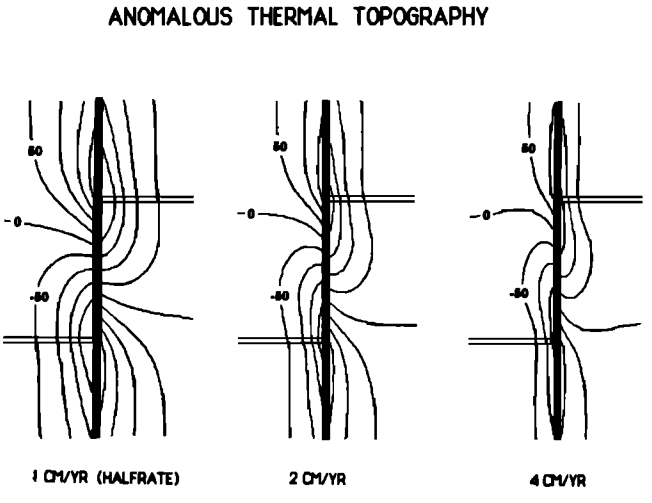

Fig. 5. Anomalous thermal topography (relative to two-dimensional plate cooling topography away from transform fault) produced by local isostatic compensation of mantle density variations due to temperature effects of transform fault. Contour lines are at 50-m intervals. Calculations are for a transform offset of 100 km and half-spreading rates of 1, 2, and 4 cm/yr.

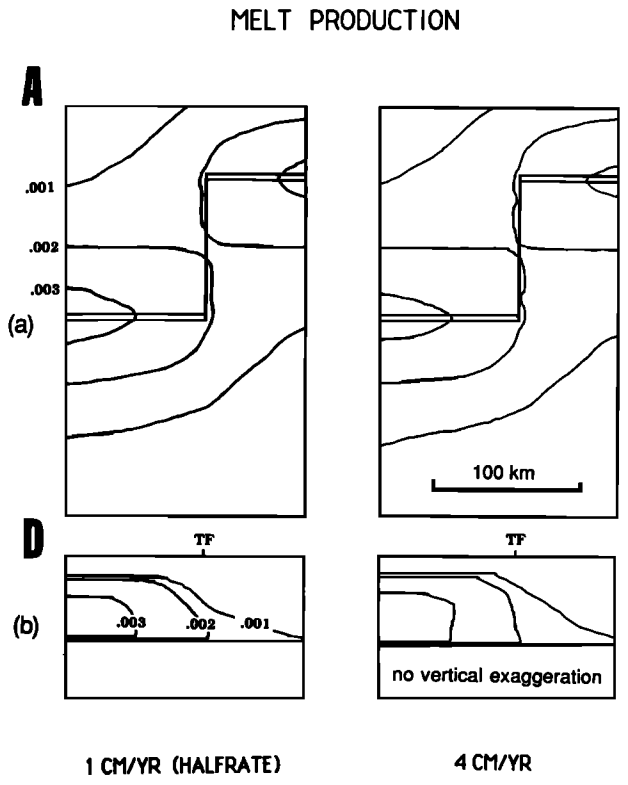

Fig. 6. Melt production rate beneath a ridge-transform-ridge spreading center for half-spreading rates of 1 and 4 cm/yr and a transform offset of 100 km. Shown are spreading center cross sections (a) at 60-km depth beneath the spreading center surface (slice A in Figure 1) and (b) a vertical cross section along a ridge axis and across to the old side of the transform fault (slice D in Figure 1). Melt production rate is normalized by the spreading rate U (i.e., the volume of melt production within a given mantle region of volume ΔV during a time Δt is our normalized melt production rate times $U\Delta V\Delta t$).

melting, ignoring the fact that the latent heat of melting will depend slightly on pressure as well as on the melt composition. The more important pressure-dependent effect that we neglect here is the experimentally observed compositional dependence of the melt eutectic on pressure [cf. *Yoder*, 1976, p. 132]. We also assume that melting is an adiabatic process. Then, after first solving for mantle temperatures assuming no melting occurs (our earlier thermal calculations), for regions in which the mantle temperature is above a pressure governed solidus given by T_m = 1100°C + z 3.25°C/km, we can find the melt production rate $\dot{\phi}=\mathbf{V}\bullet\nabla(T\text{-}T_m)$, where V is the mantle velocity (u, v, w). The total extent of melting $\phi = (T\text{-}T_m)/600°C$, where 600°C is the temperature interval from incipient to total melting of mantle material. This melt model is analogous to the melt model used by *Reid and Jackson* [1981]. The effect of the latent heat of melting on melt fraction as a function of (calculated) mantle temperature is included in the choice of the total melting interval of 600°C. (Note that although *Reid and Jackson* [1981] modify the temperature field to try to correct for the effect of the latent heat of melting on the mantle temperatures, they do so after calculating the melt fraction in the above manner. If we express mantle temperatures above the solidus T_m as $T_m + \Delta$, this type of postcorrection will decrease temperatures above the solidus to values like $T_m + \gamma\Delta$, with $\gamma = (1 + L/c_p\Delta)^{-1} \approx 0.6$, where c_p is the mantle specific heat and L is the latent heat of melting [*Reid and Jackson*, 1981]. However, this type of postcorrection does not change the calculations or results for melt production rates and total amount of melting. In any case, we feel that the effects of heat transport through melt migration will most likely be more important than this latent heat effect on mantle geotherms.) These relations will hold if we can reasonably neglect both heat transport out of melt region through melt migration and changing melt relations as melt is removed. If not, our results may be biased toward higher extents of melting than a more complete model would predict [cf. *Sleep*, 1984]. Nonetheless, to estimate crustal thickness variations we only need to know the relative amounts of melt production at a given depth. Melt production ratios will be less sensitive than absolute amounts of melt production to how much heat is transported through melt migration. This is fortunate, since melt migration is a potentially important mechanism for heat transport, as a 1% melt fraction moving at 1 m/yr will transport as much heat as its associated mantle matrix moving at 1 cm/yr, since the heat capacity of melt and mantle matrix are roughly equal. Kinematic constraints suggest that melt migration is not the primary mechanism of heat transport in the melting region but that it becomes increasingly significant at shallower depths. For example, if all melt is eventually erupted, the ratio of the crustal thickness to the depth of the melting region gives the rough estimate of the ratio of material and heat transport out of the melting region by melt versus mantle flow (this argument suggested by N. Sleep (personal communication, 1986)). For 6-km-thick crust, at 30-km depth, roughly 20% of the heat and material transport is by melt flow. If melt flow occurs primarily by rapid melt migration heat transport by melt migration would affect our calculated isotherms, whereas if melt is largely entrained in upwelling mantle matrix, the presence of melt would not strongly alter the present thermal calculations. In any case, before we explore the complexities caused by heat transport by (rapid) melt migration, we should first understand the simpler system that is studied here. The total amount of melting, unsystem that is studied here. The total amount of melting, unlike the melt production pattern, is extremely sensitive to slight changes in the melt constants of our linear solidus. The constants in our melt model were found by trial and error, so that the average crustal thickness (melt production) away from the transform fault is 6 km for a half-spreading rate of 1 cm/yr and 8 km for a half-spreading rate of 4 cm/yr [*Reid and Jackson*, 1981].

Figure 6 shows melt production rates at our model spreading center for half-spreading rates of 1 and 4 cm/yr. The total amount of melting of a particular mantle material element is simply the integral of the melt production rate along a given mantle flow line. Figure 7 shows the extent of melting for a ridge parallel mantle cross section for half-spreading rates of 1 and 4 cm/yr. Several current paradigms about melting beneath a ridge are clearly shown in these diagrams.

First, regions of mantle melting are broadly distributed beneath a ridge and may extend more than a hundred kilometers horizontally away from a ridge axis. We must reconcile this with the observation that spreading center volcanism is largely concentrated within 10 km of the ridge axis. In order for broad zones of melt production at depth to be related to narrow zones of ridge axis volcanism, melt must migrate laterally to reach the ridge axis. This suggests that ridge axis "suction" has at least a similar effect as melt buoyancy in driving melt migration, as buoyancy forces would cause pre-

dominantly vertical melt migration and hence a broad region of ridge axis volcanism. If we try to bypass this argument by invoking lithosphere impenetrability to explain the absence of large-scale off-axis volcanism, then if lithosphere impenetrability is due to melt freezing within the lithosphere before it reaches the surface, greater extents of melting at depth are needed to produce observed crustal thicknesses. However, more complicated (but plausible) melt migration scenarios are possible where melt buoyantly rises to a certain level and is then channeled to the ridge axis by variations in mantle permeability associated with the MOR volcanic plumbing system (i.e., a relatively impermeable lithosphere may channel melt toward the ridge axis). Also, if a large fraction of buoyant melt can be trapped and constrained to move with its associated mantle matrix then melt buoyancy forces may result in a local diapiric upwelling of the mantle matrix beneath a spreading center which will also tend to constrict melt (and associated matrix) upwelling to a narrow region about the ridge axis [*Rabinowicz et al.*, 1984]. *Rabinowicz et al.* [1984] show that a 15% trapped melt fraction may produce a ridge axis diapir if asthenosphere viscosity beneath the ridge is 10^{19} P and away from the ridge axis is 10^{21} P. Clearly a more complete model of melt and matrix flow is needed to test if it is possible to maintain this large a melt fraction beneath a ridge axis and to examine the driving forces for melt migration.

Second, Figure 7 shows significant differences in the total extent of melting experienced by residual mantle beneath a transform fault versus beneath the center of a spreading segment and indicates that strong lateral heterogeneities in upper mantle composition can be produced at transform offsets. However, the density variations associated with upper mantle compositional heterogeneity are not a likely cause for seafloor deepening toward a fracture zone. For example, assume that lateral density variations are causing observed deepening by Pratt isostatic compensation. Then the necessary density variation $\Delta\rho$ needed within a column of density ρ and height H to cause a topographic variation δ is $\Delta\rho = (\rho - \rho_w)\delta/(H + \delta)$, where ρ_w is the density of water. A 1 km isostatic deepening due to an increased density of the upper 30 km of mantle near a transform fault would require a 2.5% increase in upper mantle density near a transform relative to upper mantle (ρ = 3.3 g/cm^3) beneath the center of a spreading segment. While this might seem like a relatively small density contrast, if the same phases are present at equal heights within the two end-member mantle columns, this would imply a change from 10 wt % FeO and 30 wt % MgO in "undepleted" residual mantle beneath a transform to 5 wt % FeO and 35 wt % MgO in more depleted residual mantle beneath the ridge. (Here typical mantle is taken to be the mantle peridotite discussed by *Yoder* [1976, p.27].) Large differences in the total degree of melting near a transform (i.e., >25% or from 30% degree of melting beneath a ridge to 5% degree of melting beneath a transform) with a FeO depleted mantle residue are required to produce such a large residual mantle compositional change assuming that FeO/MgO partitioning follows a Forsterite-Fayalite enrichment trend [*Yoder*, 1976, p. 14]. Our calculations suggest that variations in total melting beneath a ridge are less than this, with perhaps a change from 25% total melting beneath a ridge to 10-15% melting beneath a transform fault.

Crustal thickness variations appear to be a more likely cause for seafloor deepening toward a fracture zone. A 4-km crustal thickness variation, if isostatically compensated, could produce the observed seafloor deepening. If uncompensated, only a 1-km crustal thickness variation is needed. While melt production is somewhat reduced near a transform fault (see Figure 6), it is not strongly reduced, and ridge axis upwelling induced melting may extend for tens of kilometers beneath old lithosphere across the transform fault. To investigate the feasibility of crustal thinning to produce observed deepening, we must now consider two distinct subproblems: where is melt produced beneath a ridge axis (done above) and along what path does melt migrate to its final crustal resting place? As noted above, large-scale lateral melt migration probably occurs beneath a ridge axis. Thus melt migration patterns may play a more critical role than melt production patterns in causing lateral crustal thickness variation along a ridge axis.

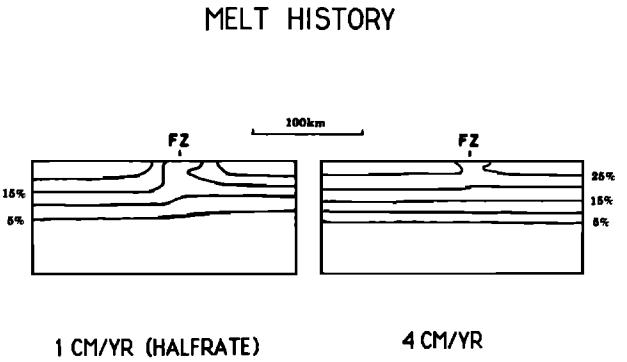

Fig. 7. Total amount of melting experienced by upper mantle beneath a spreading center. Shown are two ridge parallel vertical cross sections at the oldest part (far edge or x = -200 km) of our study region for half-spreading rates of 1 and 4 cm/yr. The fracture zone location is marked FZ.

MELT MIGRATION

To obtain a qualitative understanding of ridge axis processes, we will consider melt migration within a mantle matrix to be a porous flow problem [cf. *Ahearn and Turcotte*, 1979]. Melt migration within the mantle is inherently a two-phase reactive flow problem. *McKenzie* [1984] has recently developed in a petrological context the basic differential relations governing this two-phase flow problem. Fortunately, *Ribe* [1985] has shown that for most geological problems in melt production and melt migration a simple D'Arcy law pressure-flux relation $\mathbf{q} = -k\nabla P$ adequately describes the basic forces driving melt migration, where P is pressure, k is the matrix (mantle) permeability, and $\mathbf{q}$ ($\mathbf{q} = q_x, q_y, q_z$) is the melt flux (flow/unit area) relative to the mantle. This D'Arcy flow law is applicable, since the additional stresses associated with mantle deformation only affect melt migration by shaping the pressure distribution P; the non-D'Arcy law effects are negligible [*Ribe*, 1985]. Melt is conserved during melt migration: the net change in the melt entering and leaving a reference volume equals the melt production (or removal) in the volume or $\nabla\bullet\mathbf{q} = \dot{\phi}$ when the melt fraction (porosity) does not change with time, where $\dot{\phi}$ is the melt production rate. Combining the D'Arcy melt pressure-flux relation with this statement for melt conservation results in a Poisson equation for the melt pressure. Despite the apparent simplicity of this flow relation, there are still some fundamental uncertainties in addressing this problem, as k, the mantle permeability, depends on the fraction of melt present (and perhaps other variables as well) in a poorly known manner [cf. *McKenzie*, 1984]. In addition, the above relations implicitly require the matrix as well as melt velocity to depend on the size of the melt fraction, although for small melt fractions, mantle flow will be relatively unaffected by the presence of melt. We will ruthlessly over-

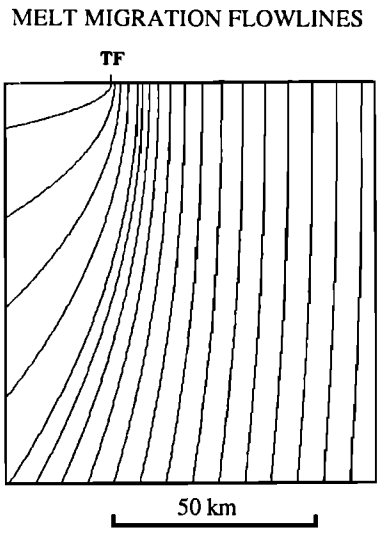

Fig. 8. Melt migration flow lines for the analytical solution for flow into a half-infinite sink discussed in the text. Shown are melt flow lines for a vertical cross section along a ridge axis and across to the old side of the transform fault (marked TF). No vertical exaggeration.

simplify the melt migration problem by assuming mantle permeability to be constant and neglecting melt wall-rock interaction on the final melt composition. If mantle permeability is a strong function of the melt fraction present in the mantle matrix, then lateral melt migration would preferentially occur at the major melting depths beneath a ridge axis and melt would migrate vertically upward only directly beneath the ridge axis. This may be a way to reconcile the observed paucity of off-axis volcanism with the possibility that melt production occurs large lateral distances away from the ridge axis.

Two simple models of melt migration will be considered here to explore the range of crustal structure that may be reasonably expected from melt migration processes. In these models we assume that the reason for the absence of large-scale off-axis volcanism is that melt migration is largely controlled by ridge axis "suction". Since we ignore the effects of melt buoyancy which tend to drive melt vertically, we are modeling the maximum effect of a ridge axis crustal sink on melt migration processes. In these models the major influences on crustal structure at the ridge axes are the ridge axis boundary conditions and the geometry of the melt production regions beneath the ridge-transform system. We use the melt production patterns from our previous calculations and two end-member ridge axis boundary conditions to model the plausible range of crustal thickness variations that may be created by melt migration processes.

The first model assumes that crustal extension at the ridge axis creates a uniform strength ridge axis sink, forcing melt migration within a uniform porosity (permeability) upper mantle matrix beneath the spreading center. In this case the flow migration pattern is found by superimposing two half-infinite line sink solutions with an offset of 100 km and is

$$u = -x(1 - y/s)/(x^2 - z^2) - x_2(1 - y/s_2)/(x_2^2 - z^2)$$
$$v = -1/s + 1/s_2$$
$$w = -z[(1 - y/s)/(x^2 - z^2) + (1 - y/s_2)/(x_2^2 - z^2)] \quad (1)$$
$$s = (x^2 + y^2 + z^2)^{1/2} \qquad s_2 = (x_2^2 + y^2 + z^2)^{1/2}$$
$$x_2 = x\text{-}100$$

where u, v, w are the magma flow velocities in the x, y, z directions. Because the transform fault spacing of 400 km is 4 times larger than the transform offset or the maximum depth of our study region, within 100 km of the transform offset this solution is practically identical to the algebraically more complicated solution for a periodic ridge axis geometry, which can be obtained, as was the above solution, by superimposing solutions for flow into a point sink [*Batchelor*, 1967, p. 89]. Figure 8 shows a vertical cross section along a ridge axis of melt migration flowlines beneath a ridge-transform spreading center. Melt produced beneath a transform fault has the clear potential to migrate tens of kilometers horizontally toward the center of a spreading segment before it reaches the surface and is emplaced to form the crust. If we assume that melt produced beneath the ridge axis follows these calculated melt flow lines to the surface, then applying this melt migration model to our calculated melt production distributions within the upper mantle predicts the crustal thickness distributions for half-spreading rates of 1 and 4 cm/yr shown in Figure 9. While too much physics is missing from this model to wholeheartedly accept these curves at face value (melt migration flow lines will be

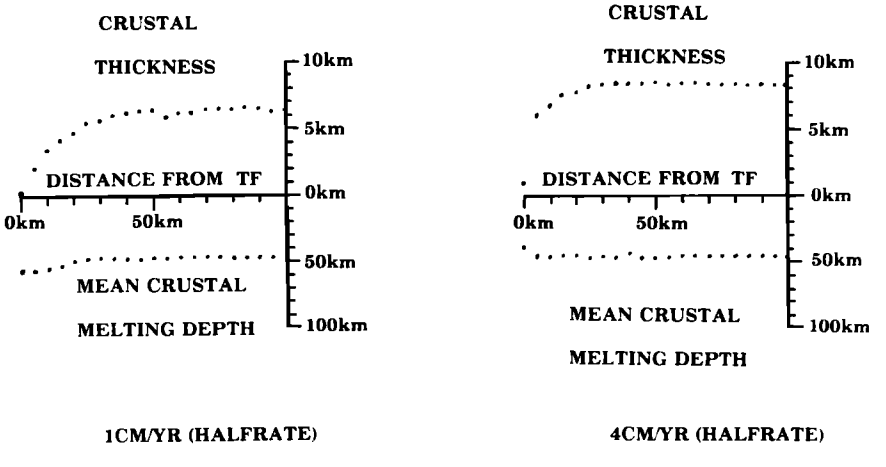

Fig. 9. Crustal thickness distribution and mean depth of melting as a function of ridge axis position for half-spreading rates of 1 and 4 cm/yr. Significant crustal thinning occurs within 30 km of the transform fault (y = 0), particularly at slow (1 cm/yr) spreading rates.

somewhat affected by the geometrical distribution of melt production), several trends are quite interesting. First, several kilometer crustal thickness variations are possible within roughly 30 km of a transform offset. The scale and amplitude of these crustal thickness variations are exactly those needed to generate observed seafloor deepening toward a fracture zone. Second, *Bender et al.*'s [1984] geochemical analysis of erupted basalts at the intermediate spreading rate Tamayo ridge-transform offset suggests that the mean melting depth is greater near the center of a spreading segment than near the transform fault. While we found that our calculated melt production distribution suggests the opposite of this trend, melt migration tends to displace melt generated deep beneath a transform fault toward the center of a spreading segment more than it displaces melt generated at shallow depths beneath a transform fault. In this way, melt migration can cause the trend described by *Bender et al.* [1984]. Figure 9 also shows the mean depth of melting of ridge axis crust as a function of ridge axis position for half-spreading rates of 1 and 4 cm/yr. In both of these calculations the trend due to the greater mean depth of melt production beneath the transform and old lithosphere across the transform (see Figure 8) overpowers the trend due to melt migration. If melting occurs at shallower depths than assumed in our model, then the effects of melt migration may dominate, producing the trend seen by *Bender et al.* [1984]. Regarding *Bender et al.*'s [1984] observations, all we can definitely say is that the effect they see, if not caused by complex shallow level processes, is probably caused by variations in melt migration near a ridge axis offset. The effect they see is not consistent with simple geophysical models for the variation in melt production at a ridge-transform intersection, which predict a shallower mean depth of melting beneath the center of a spreading segment than beneath a transform fault.

The second model for melt migration assumes that the pressure at the base of the crustal accretion zone is independent of ridge axis position, and that crustal thickness varies spatially to maintain this pressure equilibrium. If significant along-axis shallow level magma migration does occur, then along-axis variations in ridge axis pressure at the crust-mantle interface would tend to drive along-axis flow that, in turn, would tend to reduce the along-axis pressure gradients at the crust-mantle interface. In this model we assume that along-axis magma flow has resulted in zero horizontal pressure gradient along the ridge axis. We explicitly include our previously calculated melt production distribution as magma sources and the ridge axis as a variable strength sink subject to the above pressure boundary condition. Upper mantle melt permeability is again assumed to be constant, and all melt is assumed to ultimately erupt at the ridge axis so that there is no melt flow out of the rest of the spreading center system.

We solve this melt migration problem using finite difference techniques on a uniform three-dimensional grid. This problem is mathematically identical (Poisson's equation) to a heat conduction problem with heat sources and sinks, and so our thermal model described in Appendix B could be readily adapted to solve for melt pressure and flow velocities. Solutions to this model show the same form of crustal thinning as the previous model but in a more muted form. Maximum crustal thinning is roughly 1 km near the transform fault. Crustal thinning occurs within 25-30 km of the transform fault, and melt migration again tends to displace the apparent mean depth of melting to greater depths toward the center of a spreading segment than near the transform fault. Perhaps smaller amounts of melting beneath or near the transform result in a smaller permeability relative to the center of the ridge segment. This could enhance the along-axis variability that we see in this model.

Discussion

We have quantitatively developed several geophysical models to see what processes may be responsible for the TFE. Clearly, numerical and laboratory experiments must go hand in hand with observation and speculation if we are ever to obtain even rudimentary knowledge of ridge axis processes. Since little is known about the details of the processes we choose to model, we have chosen the simplest models consistent with a particular level of physical sophistication to tackle these problems. Before we attempt detailed three-dimensional models of melt segregation and migration, for example, we should have a reasonable one- or two-dimensional theoretical grasp of the relations between melt fraction and matrix permeability, and better constraints on the expected melt migration velocities beneath a ridge.

Our results suggest that transform fault induced perturbations in melt migration at a mid-ocean spreading center and transform induced perturbations on ridge axis upwelling controlled melt production are the most likely causes of the TFE. Lateral conduction of heat into the cold lithosphere abutting a ridge axis does not produce strong temperature anomalies at the mantle depths that we predict most ridge axis melting will occur; thus the thermal effects of a transform offset do not strongly affect ridge axis melting near a transform fault. Instead the major influence of a transform offset on melting beneath a ridge-transform spreading center is due to the muting effect of a transform offset on upwelling beneath the ridge-transform intersection; lower rates of upwelling lead to lower amounts of melt production within a broad region near the transform. The melt region may extend, however, for tens of kilometers across the vertical plane of the transform fault/fracture zone.

Melt migration may also affect crustal composition in ways that we have not explicitly considered. Increased shallow level upper mantle cooling near a transform offset may result in a more effective barrier to melt ascent near a transform fault. This might result in a large component of MOR crust near a transform being emplaced through along-axis crustal level magma migration (and along-axis fractionation) toward the transform fault. A subareal analog to this process has been observed in Iceland at Krafla [*Bjornsson et al.*, 1979; *Einarsson and Brandsdottir*, 1980]. However, while shallow level along-axis dike injection and magma migration from discrete volcanic centers along a ridge axis may contribute to crustal variability at a spreading center, *Bender et al.* [1984] noted that the predicted fractionation trends due to along-axis shallow level magma flow are significantly different from TFE trends, which in the Tamayo region at least, are indicative of different average melting processes or different melt source depths for basalts erupted near and far from a transform. Of course, these petrological constraints are somewhat nonunique, and more complicated models including wall-rock assimilation and magma mixing might, after suitable contortions, allow shallow level along-axis flow to be responsible for TFE compositional variability. *Mutter and Detrick*'s

[1984] seismic reflection profile across the Blake Spur fracture zone suggests that layer 1 and layer 2 thicknesses (pillow basalts and sheeted dikes) may be relatively constant while the crustal thickness changes. Most crustal thinning in their interpretation is due to a variable thickness cumulate layer 3. Thus crustal thickness changes may still reflect differences in (cumulate forming) magma supply from below the ridge even if upper crustal layers are often emplaced through along-axis dike propagation.

These models also bring into question what is meant by "typical" oceanic crustal thickness. The total crustal production along a ridge with a transform offset is always less than if no transform were present, as the broadened zone of slower upwelling associated with a transform offset will always result in less melt production near a transform offset with no compensating increase in melt production away from the transform. Further study is needed to test how strongly the reduction in melt production depends on the length of the transform offset. However, if crustal thicknesses are smoothed at a ridge axis by along-axis melt migration, then the most apparent effect of a series of small transform offsets may be regional crustal thinning. This effect, as well as spreading rate dependent differences in melt production, may be responsible for the observed 0.5-2 km differences in crustal thickness at the East Pacific Rise and Mid-Atlantic Ridge [*Reid and Jackson*, 1981].

Transform offsets may also strongly influence the spacing of volcanic centers along a spreading segment. Volcanic centers may preferentially be located toward the midpoints of spreading segments where upwelling rates and (upwelling controlled) melt production rates are highest. This effect occurs even in the absence of buoyancy forces and may more simply explain effects previously attributed to diapiric upwelling beneath the center of a spreading segment [*Schouten et al.*, 1984; *Crane*, 1985]. However, for a transform offset to have a strong influence on mantle upwelling in the melt production region, the transform offset length must be comparable to or larger than the depth of the melt region.

In many ways this paper is a reconnaissance study of the possible effects of the three-dimensional spreading geometry at a ridge-transform-ridge spreading center. We examined many processes that may affect crustal and upper mantle structure at a spreading center. We believe it is necessary to understand the effects of a physical process in relatively simple systems before trying to understand more complicated expressions of this process. Thus for example, we have not considered here the effects of heat generation from viscous dissipation along the transform fault or the additional near-surface cooling expected from hydrothermal circulation, although both of these effects can be easily implemented in our thermal model. We also have considered only uniform physical properties in our models because we are interested here in seeing the three- dimensional geometrical effects in their clearest form. Thus we have neglected the effects on the mantle flow pattern of lithospheric thickening with age that may contribute a dynamic component to the along-axis deepening of the median valley toward a ridge-transform intersection [*Parmentier and Forsyth*, 1985]. A temperature-dependent mantle viscosity will also influence upwelling by tending to concentrate upwelling in the hottest, least viscous regions.

Because we are interested in processes that can produce both geochemical as well as topographic effects near a fracture zone, we also have neglected possible mechanisms of creating stress-supported along-isochron topographic deepening toward a fracture zone. For example, possibly some of the long-lived along-isochron deepening is elastically frozen along-axis deepening that persists even after the extreme faulting the lithosphere experiences during its uplift out of the median valley into the flanking crestal mountains. Similarly thermal stresses [cf. *Turcotte*, 1974; *Parmentier and Haxby*, 1986] could potentially cause downwarping near fracture zones if the lithosphere consists of strong strips separated by mechanically weak transform faults and fracture zones. Such stress-supported topography would result in neither crustal thinning nor geochemical variations near a fracture zone.

This study has raised some provocative questions. Melt migration appears to play an important role in shaping both crustal thickness and composition. To test if melt migration is truly an important process for shaping oceanic crust, more complete models of melt migration beneath a spreading center must be developed that explicitly consider a melt fraction dependent mantle permeability, melt migration driving forces, and heat transfer by melt migration. Our results also suggest that the perturbation of mantle upwelling flow at a transform offset is the primary cause of lower degrees of melting of upper mantle near a fracture zone and hence the primary cause of lateral upper mantle heterogeneity at a spreading center. Thus this study suggests that the intuitively appealing notion that in some way upper mantle cooling near a transform is responsible for the TFE may be wrong. Clearly further study is needed to test these conclusions. At least we have shown that simple geophysical processes can produce the TFE, albeit in ways we might not have expected before we did these experiments.

APPENDIX A (FLOW MODEL)

We can solve for the plate-driven flow of a uniform viscosity mantle half-space beneath a ridge-transform-ridge spreading center with arbitrary geometry via a Fourier series flow decomposition. Several tricks can be used to considerably simplify the algebra involved in the Fourier solution for a given flow component $U_{mn} \exp^{ik_m x} \exp^{ik_n y}$. Here k_m and k_n are $2\pi m/L_x$ and $2\pi n/L_y$, respectively, where L is the boundary condition periodicity in the x or y direction, and (u, v, w) are the flow velocities in the (x, y, z) direction, x being the spreading direction, y the along-axis direction, and z vertical (see Figure 1). The simplest solution for a given

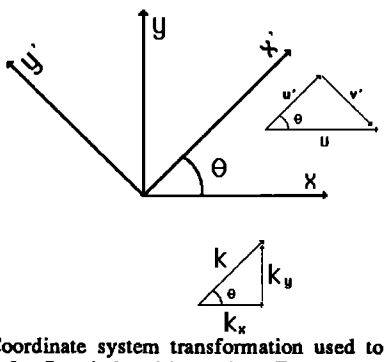

Fig. A1. Coordinate system transformation used to simplify algebraic solution for flow induced by a given Fourier component of surface motion. The surface spreading velocity U(x, y) is decomposed into u'(x', y') and v'(x', y') components for which simpler analytical solutions exist (see text for details).

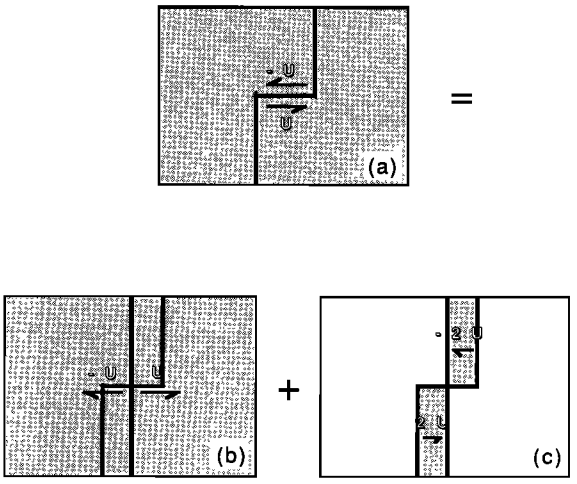

Fig. A2. Flow decomposition used in Fourier series solution. (*a*) Flow beneath a spreading center is split into two components: (*b*) Flow due to mean two-dimensional spreading center without transform offsets and (*c*) deviatoric three-dimensional flow due to geometrical deviations of a ridge-transform-ridge spreading center from the mean spreading center. This flow decomposition is primarily done for numerical convenience (see text).

$k_m k_n$ harmonic is expressible in the coordinate system rotated with respect to (x, y) by $\theta = \tan^{-1}(k_n/k_m)$ (see Figure A1). In this coordinate system the applied top surface velocity is simply expressed in terms of tangential u' (in the x' direction) and normal v' (in the y' direction) velocities that are simply a function of (cos (kx'), sin (kx')) or (cos (ky'), sin (ky')), where $k^2 = k_m^2 + k_n^2$. This algebraically simplifies the solution to a sum of two-dimensional solutions for the flow induced by surface motion in the x' and y' directions (see Figure A1). Since the solution for y' Fourier harmonics is the same as the solution for x' Fourier harmonics if we rotate x' by $\pi/2$, we will only consider flow induced by Fourier components (cos (kx'), sin (kx')) of surface flow in the x'(tangential) and y'(normal) directions. The flow induced by a given component $u'_{z=0} = (a_k \cos(kx') + b_k \sin(kx'))$ of horizontal lithosphere (top surface or $z = 0$) motion in the x' direction is

$$u' = [a_k \cos(kx') + b_k \sin(kx')]\, e^{-kz}(1 - kz)$$
$$v' = 0 \qquad \text{(A1)}$$
$$w = [a_k \sin(kx') - b_k \cos(kx')]\, kze^{-kz}$$

The flow induced by a given component $v'_{z=0} = (c_k \cos(kx') + d_k \sin(kx'))$ of horizontal lithosphere motion in the y' direction is

$$u' = 0$$
$$v' = (c_k \cos(kx') + d_k \sin(kx'))\, e^{-kz} \qquad \text{(A2)}$$
$$w = 0$$

The flow induced by an arbitrary component of top surface motion will simply be the sum of these two solutions. Thus to solve for the flow due to a given Fourier component, we solve for the flow in the (x', y', z) coordinate system and then do another coordinate transformation to rotate the solution vector back to the (x, y, z) coordinate system. A straightforward (finite) Fourier series solution to the total spreading center flow will be the solution for a problem that has periodically reflected top surface boundary conditions. Since actual plate motions are not periodically reflected, this will result in physically unreasonable flow fields near the edges of our study region and at depths comparable to the size of this region. Thus we have chosen to decompose the three-dimensional flow field into a two-dimensional spreading center centered about the mean ridge axis location plus the flow due to offsets in the ridge axis from this mean location (shown in Figure A2). The two-dimensional plate spreading has the analytical solution [*Batchelor*, 1967; *Reid and Jackson*, 1981]

$$u = 2[\tan^{-1}(x/z) - xz/(x^2 + z^2)]/\pi$$
$$w = -2z^2/\pi(x^2 + z^2) \qquad \text{(A3)}$$

So we only need to solve for the three-dimensional dipolar flow due to offsets in the ridge axis. Since this induced flow will be zero at large distances or depths from the ridge axis, it will not be affected by periodic Fourier edge effects. We use a standard FFT algorithm to solve for the flow induced by prescribed surface motions, solving equation (A1 + A2) to obtain the flow pattern at several depths beneath the spreading center. Thus the Fourier series semi-analytic technique allows us to effectively reduce the dimensionality of the problem from 3 to 2, resulting in a considerable savings in computational effort.

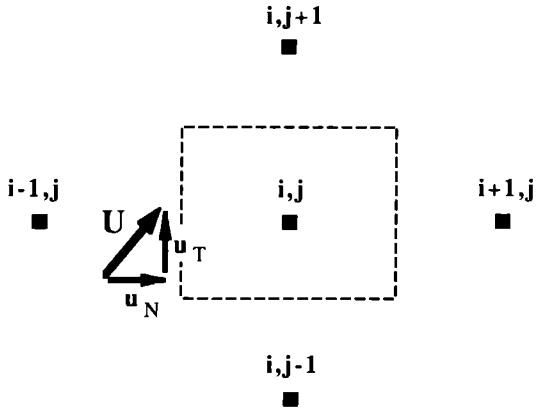

Fig. A3. A two-dimensional representation of the control volume method of generating the finite difference energy conservation equations used in our thermal calculations. Grid point temperatures approximate the mean temperature within each grid volume. Finite differences are used to calculate the heat advected and diffused into the grid volume and result in discretized equations for energy conservation within each grid (control) volume.

APPENDIX B (THERMAL MODEL)

Introduction

Finite difference techniques with a variable spacing grid were used to solve the thermal problem. The finite difference method is both easily implemented for our rectangular study region and extremely efficient in using computer memory for this memory-consuming calculation. A control volume approach with upwind differencing is used to obtain the finite difference equations. In the control volume approach [cf. *Roache*, 1982, p. 25] we consider a volume of material surrounding a grid point as shown in Figure A3. Conservation of energy for this grid volume says that in the absence of heat production (via viscous dissipation or radioactive decay, for example), the net heat advected (convected) and diffused (conducted) into and out of this volume at steady state must be zero. Using Fourier's law of heat conduction and expressing the above statement in terms of temperature for each grid

volume $\rho c_p \partial T/\partial t = 0 = \rho c_p U \bullet \nabla T + \kappa \nabla^2 T$. Using each grid point as representative average for its associated grid volume, we then discretize the above advection/conduction energy conservation equation. We choose to use upwind differences in calculating advective transport into and out of a grid volume [cf. "2nd order upwind differencing" *Roache*, 1982, p. 73]. This technique, which intuitively may be seen to account for the directional transport of advective flow, uses backward ("upwind") differences to selectively evaluate advective transport in the flow direction. Thus the heat transport q across one face of a grid volume in discretized form is:

$$q = A[u_n T_{i-1} + k(T_i - T_{i-1})] \quad u_n > 0$$
$$q = A[u_n T_i + K(T_i - T_{i-1})] \quad u_n < 0 \qquad \text{(A4)}$$

where $u_n = (u_i + u_{i-1})/2$ is the linearly interpolated velocity normal to a control volume face of area A. The engineering community has recently been in a brouhaha over the merits of upwind versus central differencing (cf. *Raithby*, [1976] for a balanced critique of upwind and central differencing). The basic advantage of upwind differencing over central differencing for advective energy transport, apart from its intuitive appeal in a control volume framework, is its numerical stability even in improperly resolved thermal boundary layers. The basic disadvantage is that this numerical stability may mask the fact that there is poor resolution in an improperly resolved boundary layer. However, this "disadvantage" is really just a statement that convergence and grid resolution studies are an essential part of a numerical experiment, even if a solution seems "converged". Several more complicated discretization upwind forms have been proposed to reduce either the numerical "crosswind" dispersion associated with flow oblique to a grid volume face or the excess numerical dissipation in upwind differencing (or deficient numerical dissipation in central differencing) compared with more complete locally exact (for one-dimensional flow) solutions for advective plus diffusive heat transport (*Brooks and Hughes* [1982] give a good discussion of these effects in a finite element context). Numerical experiments on two-dimensional grids suggest that these refinements improve the solution accuracy by <2-5% for a given problem discretization. Since these refinements, if implemented in our three-dimensional model would increase computational operations over 10-fold for a given iteration, we have chosen to use the the simple differencing forms shown above while recognizing that we perhaps will need slightly more refined grids for reasonable accuracy than we would if we used a more complex discretization treatment of advective transport.

The numerical implementation of the problem boundary conditions is straightforward. The top surface (z = 0 km) and bottom surface (z = 100 km) grid points are set to 0°C and 1310°C, respectively. On the edges of the study region, $\partial T/\partial x$ or $\partial T/\partial y$ is assumed to be zero (either because the boundary plane is a symmetry plane (transform parallel boundary plane) or because temperature variations are assumed to have a predominant vertical gradient (ridge parallel boundary plane) as expected from one-dimensional plate cooling solutions which become increasingly valid away from the ridge axis). Zero horizontal gradient temperature boundary conditions are implemented by setting the grid point temperature values on the surface to be equal to their neighboring interior grid point values after each temperature iteration (which only solves for temperatures within the grid).

In summary, the above discretization relates the temperature at each grid point to the temperature at its six nearest neighbors, resulting in a set of linear equations for the temperature at each grid point. A successive overrelaxation iterative solution technique was used to solve this system of linear equations. This equation solver minimizes the necessary computer storage to essential temperatures and velocities for each grid point, with no need to store intermediate solution values as in a direct solution technique. In each iterative sweep across the grid an updated temperature T_u is found for each grid point using the finite difference equations above. We then over-relax this updated temperature to get a new iterate solution by $T_{n+1} = T_n + \omega(T_u - T_n)$, where ω is an overrelaxation factor $1 < \omega < 2$. Convergence is much faster for overrelaxation versus relaxation ($\omega = 1$) for a well-chosen ω, which is not known a priori for this problem. We used the adaptive search method of *Hageman and Young* [1981] to find an appropriate ω (usually $1.6 < \omega < 1.9$). Sometimes the final ω chosen by this method leads to an unstable solution. In this case we used the highest stable ω found in the adaptive sequence of trial ω's as our "optimum" ω. In general one-fifth the number of iterations needed for convergence with standard relaxation ($\omega = 1$) was needed for this adaptive overrelaxation approach at a minimal cost in execution time per iteration.

Convergence and Accuracy

We used two techniques to check the accuracy of our numerical experiments. First we did standard grid refinements, solving for temperature on 63 x 41 x 23 and 32 x 21 x 12 grids for the same spreading rate and transform offset. The temperature solution, except near the ridge axis, differed by less than 1-3% for these grid discretizations, suggesting that our solution is reasonably well converged. Since greater three-dimensional grid refinement is impossible on our computer, we also used two-dimensional solutions to check the accuracy of our solution. Along-axis flow is much slower and along-axis flow gradients are much weaker than flow and flow gradients in the upwelling and spreading directions. Thus if our grid resolution can accurately capture two-dimensional spreading flow, then a similar along-axis flow discretization will accurately solve the three-dimensional problem. (We actually use a finer grid discretization in the along-axis direction.) For the two-dimensional problem we compared 63 x 23, 115 x 45, and 229 x 89 grids. The stagnation-point type flow that occurs at a ridge axis is one of the most difficult thermal problems to accurately solve, as there are both strong velocity and temperature gradients at a ridge axis. Thus we expect our solutions to be least accurate at the ridge axis and progressively more accurate away from the ridge axis. We find that the maximum temperature difference between the 63 x 23 and 115 x 45 solutions (4%) and the 115 x 45 and 229 x 89 solutions (1%) occurs roughly 7 km directly beneath the ridge axis. The temperature just beneath the ridge axis is too cool unless there are at least 15-20 points in the thermal boundary layer (229 x 89). The effect of this improper resolution of the boundary layer is to deepen the ridge axis 100° isotherms by roughly 1 km. However, more than 30 km radially away from the ridge axis (both with depth and horizontal location) the 63 x 23, 115 x

45, and 229 x 89 solutions agree to better than 10-15°C for a 1-cm/yr half-spreading rate and 15-20°C for a 4-cm/yr half-spreading rate, suggesting that our three-dimensional solutions will be accurate to 15°C away from a ridge axis and systematically over cool within 30 km of a ridge axis. Because our solutions are accurate at the major depths of melt production, we expect our three-dimensional melt production patterns to be fairly accurate, but less accurate than our temperature fields, as melt production is related to the first derivative of the temperature field (see discussion about melt production in main text). Calculated crustal thicknesses from our 63 x 23 and 229 x 89 solutions differed by 7% (1/2 km) for a 1-cm/yr half-spreading rate and by 0.4 km for a 4cm/yr half-spreading rate.

Acknowledgements: This research was supported by National Science Foundation grant OCE-8208634 and Office of Naval Research grant N00014-86-K0325. Jason Morgan suggested the flow model used in this paper (which D.W.F. developed), and Don Turcotte gave D.W.F. some helpful advice on the flow decomposition that we use. Norm Sleep provided a helpful and thought-provoking critique of this manuscript. We also thank Marc Parmentier for many helpful discussions and a review of this manuscript.

REFERENCES

Ahearn, J. L., and D. L. Turcotte, Magma migration beneath an ocean ridge, *Earth Planet. Sci. Lett.*, *45*, 115-122, 1979.

Batchelor, G. K., *An Introduction to Fluid Dynamics*, 615 pp., Cambridge University Press, New York, 1967.

Bender, J. F., C. H. Langmuir, and G. N. Hanson, Petrogenesis of basalt glasses from the Tamayo region, East Pacific Rise, *J. Petrol.*, *25*, 213-254, 1984.

Bjornsson, A., G. Johnson, S. Sigurdsson, G. Thorbergsson, and E. Tryggvason, Rifting of the plate boundary 1975-1978, *J. Geophys. Res.*, *84*, 3029-3038, 1979.

Brooks, A. N., and T. J. R. Hughes, Streamline Upwind/Petrov-Galerkin formulations for convection dominated flows with particular emphasis on the incompressible Navier-Stokes equations, *Comp. Meth. Appl. Mech. Eng.*, *32*, 199-259, 1982.

Cormier, M., R. S.Detrick, and G. M. Purdy, Anomalously thin crust in oceanic fracture zones, New seismic constraints from the Kane fracture zone, *J. Geophys. Res.*, *89*, 10,249-10,266, 1984.

Crane, K., The spacing of rift highs: Dependence on diapiric processes in the underlying asthenosphere?, *Earth Planet. Sci. Lett.*, *72*, 405-414, 1985.

Detrick, R. S., and G. M. Purdy, The crustal structure of the Kane fracture zone from seismic refraction studies,*J. Geophys. Res.*, *85*, 3759-3777, 1980.

Einarsson, P., and B. Brandsdottir, Seismological evidence for lateral magma intrusion during the July, 1978 deflation of the Krafla volcano in N.E. Iceland, *J. Geophys.*, *47*, 160-165, 1980.

Forsyth, D. W., and B. Wilson, Three-dimensional temperature structure of a ridge-transform-ridge system, *Earth Planet. Sci. Lett.*, *70*, 355-362, 1984.

Fox, P. J., and D. G. Gallo, A tectonic model for ridge-transform-ridge plate boundaries: Implications for the structure of oceanic lithosphere, *Tectonophysics.*, *104*, 205-242, 1984.

Hageman, L. A., and D. M. Young, *Applied Iterative Analysis*, 380 pp., Academic, Orlando, Fla., 1981.

Hekinian, R., and G. Thompson, Comparative geochemistry of volcanics from rift valleys, transforms and aseismic ridges, *Contrib. Mineral. Petrol.*, *57*, 145-162, 1976.

McKenzie, D. P., The generation and compaction of partially molten rock, *J. Petrol.*, *25*, 713-765, 1984.

Mutter, J. C., and R. S. Detrick, Multichannel seismic evidence for anomalously thin crust at Blake Spur fracture zone, *Geology*, *12*, 534-537, 1984.

Parmentier, E. M., and D. W. Forsyth, Three-dimensional flow beneath a slow spreading ridge axis: A dynamic contribution to the deepening of the median valley toward fracture zones, *J. Geophys. Res.*, *90*, 678-684, 1985.

Parmentier, E. M., and W. F. Haxby, Thermal stresses in the oceanic lithosphere: Evidence from geoid anomalies at fracture zones, *J. Geophys. Res.*, *91*, 7193-7204, 1986.

Phipps Morgan, J., E. M. Parmentier, and J. Lin, Mechanisms for the origin of mid-ocean ridge axial topography: Implications for the thermal and mechanical structure of accreting plate boundaries, *J. Geophys. Res.*, in press, 1987.

Rabinowicz, M., A. Nicolas, and J. L. Vigneresse, A rolling mill effect in asthenosphere beneath oceanic spreading centers, *Earth Planet. Sci. Lett.*, *67*, 97-108, 1984.

Raithby, G. D., A critical evaluation of upstream differencing applied to problems involving fluid flow, *Comp. Meth. Appl. Mech. Eng.*, *9*, 75-103, 1976.

Reid, I. D. and H. R. Jackson, Oceanic spreading rate and crustal thickness, *Mar. Geophys. Res.*, *5*, 165-172, 1981.

Ribe, N. M., The deformation and compaction of partially molten zones, *Geophys. J. R. Astron. Soc.*, *83*, 487-501, 1985.

Roache, P. J., *Computational Fluid Dynamics*, 446 pp., Hermosa Publishers, Albuquerque N.M., 1982.

Schouten, H., K. D. Klitgord, and J. A. Whitehead, Segmentation of mid-ocean ridges, *Nature*, *317*, 225-229, 1985.

Sleep, N. H., Tapping of magmas from ubiquitous mantle heterogeneities: An alternative to mantle plumes?, *J. Geophys. Res.*, *89*, 10,029-10,041, 1984.

Turcotte, D. L., Are transform faults thermal contraction cracks?, *J. Geophys. Res.*, *79*, 2573-2577, 1974.

Yoder, H. S., *Generation of Basaltic Magma*, 265 pp., National Academy of Sciences, Washington, D.C., 1976.

White, R. S., R. S. Detrick, M.C. Sinha, and M.H. Cormier, Anomalous seismic crustal structure of oceanic fracture zones, *Geophys. J. R. Astron. Soc. 79*, 779-798, 1984.

D.W. Forsyth, Department of Geological Sciences, Brown University, Providence, RI 02912.

J. Phipps Morgan, Department of Earth, Atmospheric, and Planetary Sciences, Massachusetts Institute of Technology, Cambridge, MA 02139.

(Received July 3, 1986;
revised March 1, 1987;
accepted March 17, 1987.)